

## Direct measurement of the anisotropy of the resistivity in the $a$ - $b$ plane of twin-free, single-crystal, superconducting $\text{YBa}_2\text{Cu}_3\text{O}_{7-\delta}$

T. A. Friedmann, M. W. Rabin, J. Giapintzakis, J. P. Rice, and D. M. Ginsberg

*Department of Physics and Materials Research Laboratory, University of Illinois at Urbana-Champaign,  
1110 West Green Street, Urbana, Illinois 61801*

(Received 10 May 1990)

We have measured the resistivity tensor in one nearly twin-free crystal and one twin-free crystal of  $\text{YBa}_2\text{Cu}_3\text{O}_{7-\delta}$ . The first crystal was grown with a large twin-free region. We removed the twins in the second crystal by applying a uniaxial stress. Using a modified Montgomery technique, we measured the electrical resistivities in all three crystal directions and found them to be linear in temperature above the superconducting transition temperature  $T_c$ . Our results for  $\rho_a$  and  $\rho_b$  at room temperature are among the lowest that have been reported in the literature, indicating that our samples are of high quality. The ratio  $\rho_a/\rho_b$  is independent of temperature between 150 and 275 K, and its value,  $2.2 \pm 0.2$ , indicates that the Cu-O chains contribute 60% of the current when the electric field is parallel to them, with the rest of the current being contributed by the Cu-O planes. This result, at zero frequency, is in good agreement with the recent conductivity at infrared frequencies obtained by Schlesinger *et al.*

### I. INTRODUCTION

$\text{YBa}_2\text{Cu}_3\text{O}_{7-\delta}$  is a high-temperature superconductor, and it has attracted much attention because of its unusual structure (containing Cu-O planes and chains) and its excellent properties (e.g., a sharp superconducting transition). Most measurements, including ours, have been made on material having a stoichiometry with  $\delta$  near 0.1, correlated with a superconducting transition temperature  $T_c$  in excess of 90 K. Obtaining an understanding of the normal-state properties of  $\text{YBa}_2\text{Cu}_3\text{O}_{7-\delta}$  is an important step toward understanding its superconducting properties. There have been many measurements of its resistivity in both polycrystalline and twinned single-crystal samples. In spite of these measurements, there is still doubt as to whether the  $c$ -axis resistivity,  $\rho_c$ , is linear in temperature,<sup>1,2</sup> or has an upturn near  $T_c$ .<sup>3,4</sup> Furthermore, no one has published results for the  $a$ - $b$  resistivity anisotropy,  $\rho_a/\rho_b$ , because it has been difficult to make twin-free crystals of this compound. (The  $b$  direction is parallel to the Cu-O chains in our notation.) We report measurements of  $\rho_a/\rho_b$  for a nearly twin-free crystal and a twin-free crystal, analyzed with a modified Montgomery technique.<sup>5,6</sup>

### II. SAMPLE PREPARATION

The two single crystal samples used in this study were grown by a self-flux technique, as described elsewhere.<sup>7</sup> We used yttria-stabilized zirconia crucibles instead of alumina crucibles to avoid aluminum impurities in our samples. These impurities greatly affect the  $c$ -direction resistivity.<sup>2</sup> Oxygenation was carried out during post-growth annealing in flowing  $\text{O}_2$ , first for 1 h at 600°C and then for 96 h at 400°C. This technique provides excellent single crystals, with sharp superconducting transitions.

The Montgomery method requires a sample with rectangular faces oriented parallel to the crystal axes. Our samples were rectangular, and their  $ab$  faces were nearly square; their dimensions are given in Table I. As grown, sample *A* had a large twin-free domain. It had been quenched in the tetragonal phase during crystal growth, as reported elsewhere.<sup>8</sup> We cleaved this sample along the  $a$  and  $b$  crystal axes to remove the twinned regions and leave a nearly twin-free single crystal. (Magnetization measurements on sample *A* before the contacts were put onto it are reported elsewhere.<sup>8</sup>) Though grown in the same fashion as sample *A*, sample *B* had many twins, as do 95% of all crystals grown this way. We polished this

TABLE I. Sample dimensions, linear fit parameters,  $\rho_i(T) = \alpha_i T + \beta_i$ , for  $150 \text{ K} < T < 220 \text{ K}$ , and resistivities at 100 and 275 K.

Sample	Axis	$l'$ ( $\mu\text{m}$ )	$\alpha_i$ ( $\mu\Omega \text{ cm/K}$ )	$\beta_i$ ( $\mu\Omega \text{ cm}$ )	$\rho$ ( $\mu\Omega \text{ cm}$ ) $T=100 \text{ K}$	$\rho$ ( $\mu\Omega \text{ cm}$ ) $T=275 \text{ K}$
<i>A</i>	<i>a</i>	530	0.554	-13.9	40	146
<i>A</i>	<i>b</i>	470	0.237	-2.81	21	68
<i>A</i>	<i>c</i>	24.0	12.5	1110	2300	4800
<i>B</i>	<i>a</i>	750	0.691	-13.0	53	178
<i>B</i>	<i>b</i>	865	0.269	-2.12	25	73
<i>B</i>	<i>c</i>	44.1	12.5	2220	3400	5600

crystal to a rectangular shape perpendicular to the  $a$  and  $b$  crystal axes, and removed all of its twin boundaries by applying a uniaxial stress at 450°C in flowing oxygen on the hot stage of an optical microscope having crossed polarizers, as described previously.<sup>9</sup> We examined both samples under crossed polarizers to look for twinning. One corner of sample  $A$  had a very small second twin domain in the vicinity of one contact. Sample  $B$  was untwinned. We believe, therefore, that the properties reported here for each sample were determined by a single domain.

The Montgomery analysis assumes that the sample has point contacts at the vertices of the crystal, so we made electrical contact through eight small gold pads placed as near to the corners of the  $ab$  faces as possible. We evaporated the gold pads onto the sample through a 30- $\mu\text{m}$ -diam hole in a mechanical mask. The distance from the edge of each contact to each adjacent edge of the sample was less than 10  $\mu\text{m}$ . Annealing the sample at 400°C for 48 h in flowing  $\text{O}_2$  made the gold pads stick to the surface and reduced the contact resistance from  $\sim 1 \text{ k}\Omega$  to  $\sim 1 \Omega$ .

The contact application procedure did not affect the bulk properties of our crystals. The dc magnetization of the crystals as measured in a superconducting quantum interference device magnetometer after the final heat treatment showed a very sharp ( $< 2 \text{ K}$  wide) bulk transition (Fig. 1). Secondary-ion mass spectrometry (SIMS) performed on a similarly prepared twinned crystal demonstrated that the depth of gold diffusion after such a heat treatment was  $< 0.2 \mu\text{m}$  in the  $c$  direction of the sample.

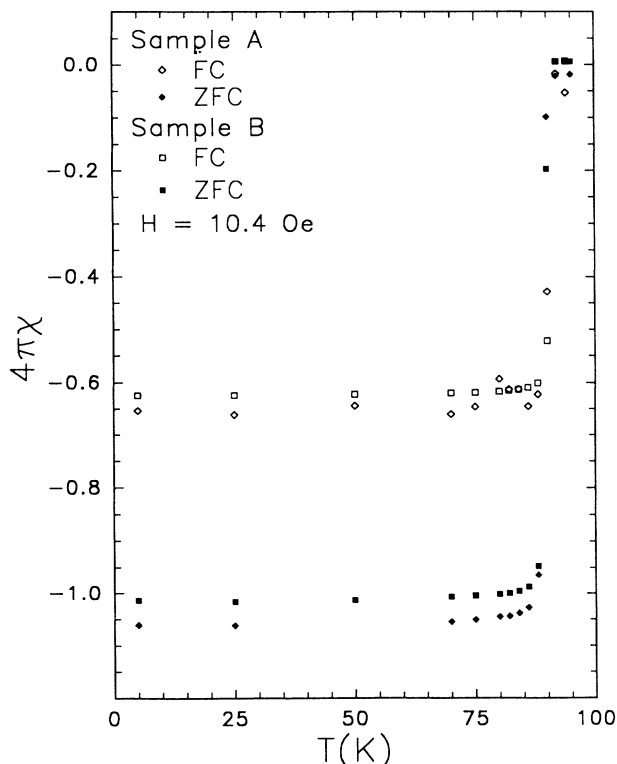


FIG. 1. Magnetic susceptibility  $\chi$  vs temperature  $T$ . Zero-field-cooled (ZFC) and field-cooled (FC) data are shown.

### III. MEASUREMENTS AND METHODS

We thermally anchored each sample to a copper grid with General Electric GE7031 varnish, allowing access to all eight corners, and we made final electrical contact to the crystals, using a micromanipulator and silver paste to attach 25- $\mu\text{m}$ -diam gold wires to the contact pads. The diameter of contact of the silver paste was approximately 50–100  $\mu\text{m}$ , larger than the 30- $\mu\text{m}$ -diam gold contact pad. No additional heat treatment was necessary to achieve low contact resistances. Since silver paste does not make good electrical contact to  $\text{YBa}_2\text{Cu}_3\text{O}_{7-\delta}$  crystals without a heat treatment, the effective contact diameter is that of the gold pad.

We monitored the sample temperature with a calibrated platinum resistor, and took data only after achieving thermal equilibrium. We stabilized the temperature to within 1 mK for  $80 \text{ K} < T < 110 \text{ K}$  and to within 10 mK for  $T > 110 \text{ K}$ .

We measured the Montgomery resistances,  $R_{ij} = V/I$ , for the configuration of leads schematically shown in Fig. 2, using a computer-controlled, calibrated ac bridge<sup>10</sup> operated at 50 Hz and a current of 600  $\mu\text{A}$ . The results were insensitive to the size of the current.  $R_{ij}$  is the resistance when the current nominally flows in the  $i$  direction and the four contacts are configured on or near the  $ij$  face. Rotating the lead configuration on the crystal by  $90^\circ$  gives the resistance  $R_{ji}$ , so we were able to measure six  $R_{ij}$  configurations: two on each of the  $ab$ ,  $bc$ , and  $ca$  faces. Ideally, only three such measurements are necessary to determine the resistivities; our six measurements overdetermine the parameters, providing a consistency check. Below  $T_c$ ,  $R_{ij}$  is apparently small but positive ( $\sim 10^{-4} \Omega$ , too small to see in Figs. 2 and 3), and independent of temperature, but varying with frequency, current, and lead configuration. This small instrumental offset was subtracted from the data. Figure 2–5 show the  $R_{ij}$  as a function of temperature.

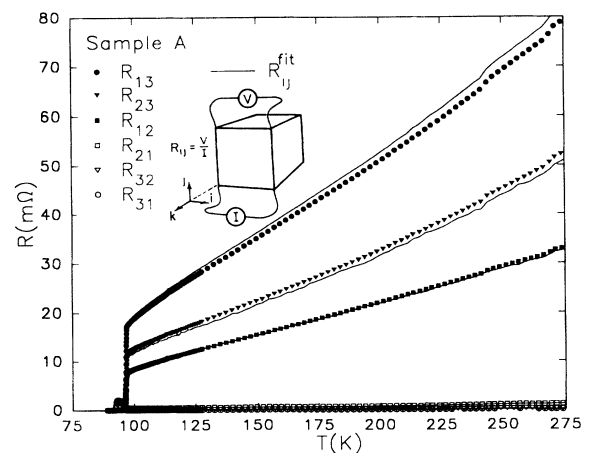


FIG. 2. Montgomery resistances  $R_{ij}$  and their fitted values  $R_{ij}^{\text{fit}}$  vs  $T$  for sample  $A$ . Note: we perform a new fit to the  $R_{ij}$  at each temperature. Inset: schematic diagram of the contact geometry on one face of the sample.

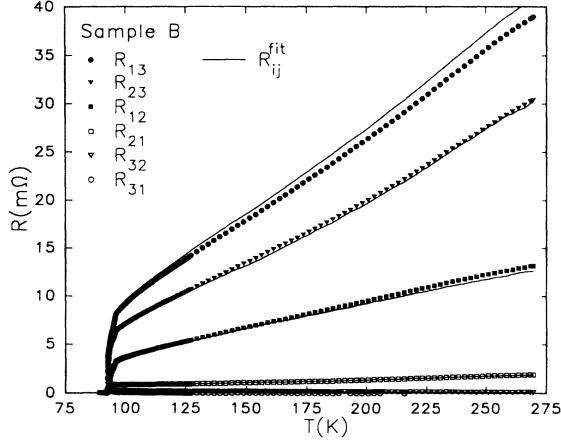


FIG. 3. Montgomery resistances  $R_{ij}$  and their fitted values  $R_{ij}^{\text{fit}}$  vs  $T$  for sample  $B$ .

#### IV. RESISTIVITY CALCULATIONS

To determine the resistivities,  $\rho_i$ , from the  $R_{ij}$  data, we combine van der Pauw's<sup>11</sup> mapping between equivalent anisotropic and isotropic crystals, Eqs. (1) and (2), with the calculation by Logan, Rice, and Wick<sup>6</sup> (LRW) of  $R_{ij}$  for an isotropic crystal, Eqs. (3) and (4). The mapping of van der Pauw,

$$l_i = l'_i \left[ \frac{\rho_i}{\rho} \right]^{1/2}, \quad (1)$$

$$\rho = (\rho_1 \rho_2 \rho_3)^{1/3}, \quad (2)$$

determines the dimensions,  $l_i$ , and resistivity,  $\rho$ , of an isotropic crystal that has the same  $R_{ij}$  values as a rectangular crystal with edges aligned with the principal axes of the resistivity tensor and having the lengths  $l'_i$ . For such an isotropic crystal, LRW found

$$R_{ij} = \frac{8l_j \rho}{l_i l'_k} \sum_{m=1, \text{ odd}}^{\infty} \sum_{n=0}^{\infty} \frac{\epsilon_n}{S_{ijmn} \sinh(S_{ijmn})}, \quad (3)$$

where  $\epsilon_0 = 1$ ;  $\epsilon_n = 2$  for  $n \neq 0$ ;  $i, j$ , and  $k$  are distinct, and

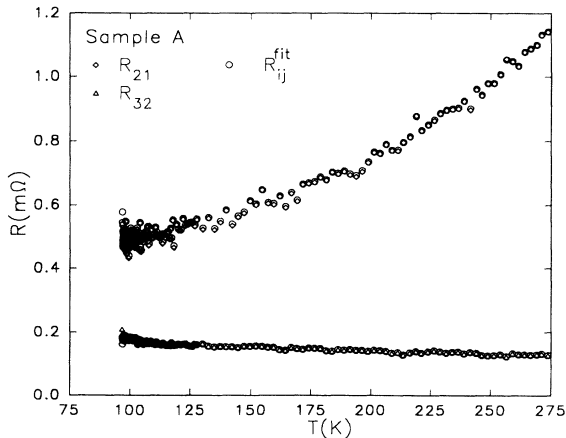


FIG. 4. A magnification of part of Fig. 2.

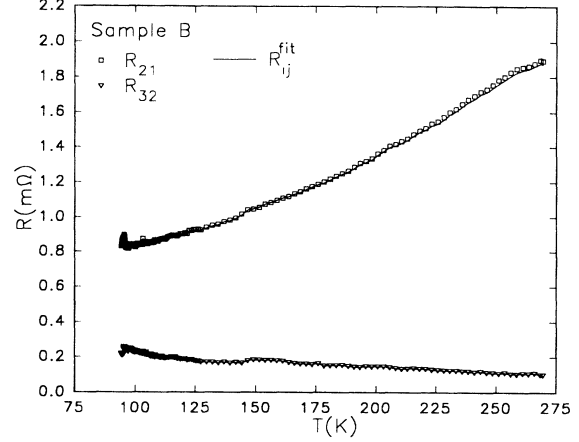


FIG. 5. A magnification of part of Fig. 3.

$$S_{ijmn}^2 = \pi^2 m^2 \left[ \frac{l_j}{l_i} \right]^2 + \pi^2 n^2 \left[ \frac{l_j}{l_k} \right]^2. \quad (4)$$

Substituting van der Pauw's mapping into the LRW formulas, we find

$$R_{ij} = \frac{8l'_j \rho_j}{l'_i l'_k} \sum_{m=1, \text{ odd}}^{\infty} \sum_{n=0}^{\infty} \frac{\epsilon_n}{S_{ijmn} \sinh(S_{ijmn})}, \quad (5)$$

$$S_{ijmn}^2 = \pi^2 m^2 \left[ \frac{l'_j}{l'_i} \right]^2 \left[ \frac{\rho_j}{\rho_i} \right] + \pi^2 n^2 \left[ \frac{l'_j}{l'_k} \right]^2 \left[ \frac{\rho_j}{\rho_k} \right]. \quad (6)$$

We must find the resistivities,  $\rho_i$ , that satisfy these equations.

By performing a nonlinear, least-squares fit to the  $R_{ij}$  values, using a modification of the implementation of Press *et al.*<sup>12</sup> of the Levenberg-Marquardt algorithm, we computed a different set of resistivities ( $\rho_a, \rho_b, \rho_c$ ) at each temperature. Our computations iteratively reduce the sum of the squares of the fractional deviations of the fit from the data:

$$\chi^2 = \sum \left[ \frac{(R_{ij}^{\text{fit}} - R_{ij})}{R_{ij}} \right]^2. \quad (7)$$

The sum is over the data points, at each temperature. By weighting the  $R_{ij}$  values equally, this form of  $\chi^2$  preserves the significance of all the data, regardless of their magnitudes; this is crucial because our data span up to five decades at a given temperature. In fitting the measurements, we chose to discard the  $R_{31}$  points because the signal to noise ratio was too low. Figure 6 and 7 show the calculated resistivities.

Our use of a fitting algorithm and the three-dimensional  $R_{ij}$  formulas, Eqs. (5) and (6), deviates from the analysis of Montgomery. His method demands (a) that two of the resistivity tensor's eigenvalues be degenerate, (b) that the crystal be electrically thick [ $l_k \gg (l_i l_j)^{1/2}$ ] or thin [ $l_k \ll (l_i l_j)^{1/2}$ ], or (c) that we ignore the variation of  $R_{ij}/R_{ji}$  with  $l_k$ . Our goal is to

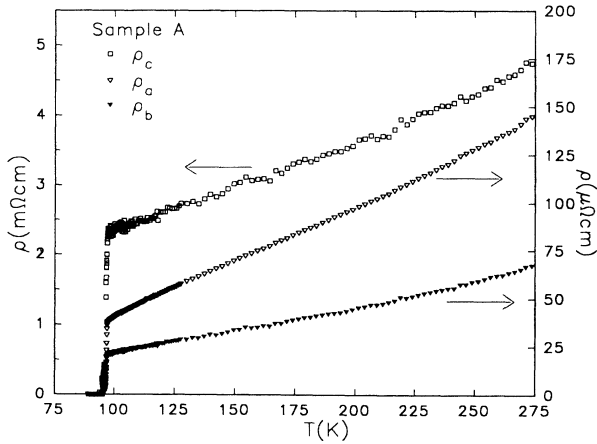


FIG. 6. The resistivity tensor's eigenvalues  $\rho_a$ ,  $\rho_b$ , and  $\rho_c$  vs  $T$  for sample  $A$ . The values of  $\rho_c$  are not precisely determined; see the text.

differentiate between resistivities in all three directions, and our samples are not electrically thick or thin for all contact configurations. Though in a first approximation we can ignore the variation of  $R_{ij}/R_{ji}$  with  $l_k$  and use calibration curves as Montgomery did, it is more precise to make a three-dimensional calculation. Additionally, we have more than the minimum number of data to determine the  $\rho_i$  values, and an examination of  $\chi^2$  provides us with a simple consistency check.

Both data sets indicate that the superconducting transition begins near 96 K; the zero-resistance temperature was near 92 K. The fits to the data below 96 K were not good for sample  $A$ , with large  $\chi^2$  values. Similarly bad  $\chi^2$  values occurred for sample  $B$  but below 94 K. The reason for this deviation is unknown; probably the samples are electrically less homogeneous near  $T_c$ . The data for  $T > 96$  K were fitted to within 2% with small systematic deviations, as can be seen in Figs. 2–4. The systematic deviations seen there could be caused (a) by sample inhomogeneity or (b) by nonideal contacts of finite area, slightly displaced from the corners. The value of  $\rho_c$

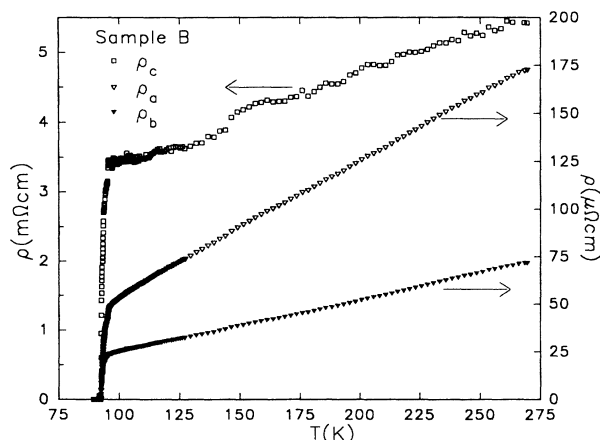


FIG. 7. The resistivity tensor's eigenvalues  $\rho_a$ ,  $\rho_b$ , and  $\rho_c$  vs  $T$  for sample  $B$ . The values of  $\rho_c$  are not precisely determined; see the text.

is critically dependent on  $R_{32}$  because  $R_{32}$  is the only configuration used in the fit for which the current is principally in the  $c$  direction. (The noise in the data for  $R_{32}$  is directly seen in the  $\rho_c$  versus  $T$  plots of Figs. 6 and 7.) Any systematic errors in the data for  $R_{32}$  are transformed into errors in  $\rho_c$ . The magnitude of  $R_{32}$  is small because the crystals are thin. Thus, our values of  $\rho_c$  are not very precise and should not be used in place of those already published by other groups on samples with more favorable shapes. It should be noted that our results for  $\rho_a$  and  $\rho_b$  are not very sensitive to the value of  $\rho_c$  because the samples are thin. The total uncertainties in the calculated values of  $\rho_a$  and  $\rho_b$  in each sample appear to be less than the variation from sample  $A$  to sample  $B$ .

## V. RESULTS

Figure 8 shows the anisotropy ratio  $\rho_a/\rho_b$  for both samples. We conclude that the  $\rho_a/\rho_b$  anisotropy is  $2.2 \pm 0.2$  between 150 and 275 K. The enhanced conductivity in the  $b$  direction shows the influence of the Cu-O chains.

Our results for  $\rho_a$  and  $\rho_b$  at room temperature are among the lowest that have been reported in the literature, indicating that our samples are of high quality. At room temperature  $\rho_c \approx 5.3$  m $\Omega$  cm, which is lower than the range of 8–20 m $\Omega$  cm reported by others,<sup>2–4</sup> but this is the direction for which the uncertainty in our results is large. We can compare  $\rho_c/\rho_a$  and  $\rho_c/\rho_b$  to the measurements of  $\rho_c/\rho_{ab}$  by other groups, where  $\rho_{ab}$  is the planar resistivity in twinned crystals. Their values range from 30 to 100 at room temperature and 52 to 250 at 100 K.<sup>2–4</sup> At 275 K, we find  $\rho_c/\rho_a \sim 35$  and  $\rho_c/\rho_b \sim 75$ , while at 100 K,  $\rho_c/\rho_a \sim 63$  and  $\rho_c/\rho_b \sim 120$ , within the previously published ranges of values.

The resistivities in all three directions are linear in temperature. Table I summarizes the fits of the resistivities to linear functions of temperature  $\rho_i(T) = \alpha_i T + \beta_i$  for  $150 \text{ K} < T < 220 \text{ K}$  for each crystal. The intercepts for  $\rho_b(T)$  are nearly zero for both samples, since  $\beta_b \approx -2.5$   $\mu\Omega$  cm, while those for  $\rho_a(T)$  are both negative, with  $\beta_a \approx -13.5$   $\mu\Omega$  cm. As shown in Figs. 6 and 7, when  $T$  is

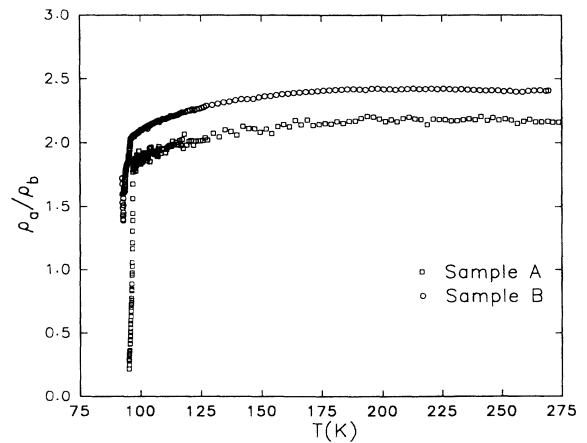


FIG. 8. Resistivity ratio  $\rho_a/\rho_b$  vs  $T$  for samples  $A$  and  $B$ .

reduced toward  $T_c$ ,  $\rho_a$  deviates from linearity in a manner indicating fluctuations of small regions of the sample into the superconducting state. This type of deviation is also seen for  $\rho_b$ , but is smaller in magnitude. The resistivities deviate from linearity above 240 K, possibly indicating anomalous behavior near that temperature, as seen in many other types of experiments.<sup>13,14</sup>

By taking the geometric mean of  $\rho_a$  and  $\rho_b$  at room temperature, we can calculate an effective in-plane resistivity for our twin-free samples;  $\rho_{ab} = (\rho_a \rho_b)^{1/2} = 110 \mu\Omega \text{ cm}$ . This value falls below those of the best twinned crystals,  $\rho_{ab} = 150$  to  $250 \mu\Omega \text{ cm}$ ,<sup>2-4,15</sup> indicating that twin boundaries significantly increase the planar resistivities.

The resistivity in the  $b$  direction is significantly less than that in the  $a$  direction. Naively, we separate the chain conductivity from the plane conductivity. Assuming that the  $a$  direction conductivity is the intrinsic plane conductivity and that the  $b$  direction conductivity contains contributions from both the planes and the chains, we have

$$\begin{aligned}\sigma_b &= \sigma_{\text{chain}} + \sigma_{\text{plane}}, \\ \sigma_a &= \sigma_{\text{plane}}.\end{aligned}\quad (8)$$

This gives for the chain and plane conductivity at room temperature:

$$\begin{aligned}\sigma_{\text{chain}} &= 0.0084 (\mu\Omega \text{ cm})^{-1}, \\ \sigma_{\text{plane}} &= 0.0056 (\mu\Omega \text{ cm})^{-1}, \\ \frac{\sigma_{\text{chain}}}{\sigma_{\text{chain}} + \sigma_{\text{plane}}} &= 0.60.\end{aligned}\quad (9)$$

Far-infrared measurements were recently made by Schlesinger *et al.*<sup>16</sup> on twin-free samples of  $\text{YBa}_2\text{Cu}_3\text{O}_{7.8}$ . The data indicate that 50–60% of the infrared conductivity is associated with the chains. This agrees well with our result of 60%. It should be noted, however, that Schlesinger *et al.* extrapolate their conductivity measurements to zero frequency and find that the  $a$ - $b$  anisotropy would be only 10–30%, whereas we find  $\rho_a/\rho_b = 2.2 \pm 0.2$ . The extrapolation to zero frequency is difficult, in our opinion.

## VI. CONCLUSIONS

We have measured the anisotropy of the resistivity in twin-free single crystals of  $\text{YBa}_2\text{Cu}_3\text{O}_{7.8}$ . The dc anisotropy ratio  $\rho_a/\rho_b$  has been determined for the first time. Between 150 and 275 K, the anisotropy ratio  $\rho_a/\rho_b$  is temperature independent and is equal to  $2.2 \pm 0.2$ . This result is in good agreement with the recent infrared conductivity data of Schlesinger *et al.*

## ACKNOWLEDGMENTS

This research was supported in part by the National Science Foundation (NSF) Grant Nos. 87-14555 (T.A.F., D.M.G., and J.P.R.), 89-20538 (J.G.), and (through the Science and Technology Center for Superconductivity) STC-88-09854 (M.W.R.). Judith E. Baker, in the Materials Research Laboratory's Center for Microanalysis of Materials, performed the SIMS analysis of the diffusion of gold from the contact pads into the sample; that work was supported by Department of Energy Contract No. DE-AC-02-76ER-01198.

- <sup>1</sup>Y. Iye, T. Tamegai, T. Sakakibara, T. Goto, N. Miura, H. Takeya, and H. Takei, *Physica C* **153-155**, 26 (1988).  
<sup>2</sup>G. Weigang and K. Winzer, *Z. Phys. B* **77**, 11 (1989).  
<sup>3</sup>S. J. Hagen, T. W. Jing, Z. Z. Wang, J. Horvath, and N. P. Ong, *Phys. Rev. B* **37**, 7928 (1988).  
<sup>4</sup>S. W. Tozer, A. W. Kleinsasser, T. Penney, D. Kaiser, and F. Holtzberg, *Phys. Rev. Lett.* **59**, 1768 (1987).  
<sup>5</sup>H. C. Montgomery, *J. Appl. Phys.* **42**, 2971 (1971).  
<sup>6</sup>B. F. Logan, S. O. Rice, and R. F. Wick, *J. Appl. Phys.* **42**, 2975 (1971).  
<sup>7</sup>J. P. Rice, B. G. Pazol, D. M. Ginsberg, T. J. Moran, and M. B. Weissman, *J. Low Temp. Phys.* **72**, 345 (1988).  
<sup>8</sup>J. P. Rice, D. M. Ginsberg, M. W. Rabin, K. G. Vandervoort, G. W. Crabtree, and H. Claus, *Phys. Rev. B* **41**, 6532 (1990).  
<sup>9</sup>J. Giapintzakis, D. M. Ginsberg, and P.-D. Han, *J. Low Temp. Phys.* **77**, 155 (1989).

- <sup>10</sup>J. R. Matey, S. B. Dierker, and A. C. Anderson, *Rev. Sci. Instrum.* **50**, 641 (1979).  
<sup>11</sup>L. J. van der Pauw, *Philips Res. Rep.* **16**, 187 (1961).  
<sup>12</sup>W. H. Press, B. P. Flannery, S. A. Teukolsky, W. T. Vetterling, *Numerical Recipes in Pascal* (Cambridge University Press, Cambridge, U.K., 1989).  
<sup>13</sup>D. C. Johnston, S. K. Sinha, A. J. Jacobson, and J. M. Newsam, *Physica C* **153-155**, 572 (1988).  
<sup>14</sup>K. Fosshem, O. M. Nes, T. Laegrid, C. N. W. Darlington, D. A. O'Connor, and C. E. Gough, *Int. J. Mod. Phys. B* **2**, 1171 (1988).  
<sup>15</sup>T. A. Friedmann, J. P. Rice, J. Giapintzakis, and D. M. Ginsberg, *Phys. Rev. B* **39**, 4258 (1989).  
<sup>16</sup>Z. Schlesinger, R. T. Collins, F. Holtzberg, C. Feild, S. H. Blanton, U. Welp, G. W. Crabtree, Y. Fang, and J. Z. Liu, *Phys. Rev. Lett.* **65**, 801 (1990).